Giant Raman enhancement on nanoporous gold film by conjugating with nanoparticles for single-molecule detection†

Lihua Qian,[a] Biswajit Das,*[a] Yan Li[b] and Zhilin Yang*[b]

Received 30th March 2010, Accepted 3rd June 2010
DOI: 10.1039/c0jm00884b

Hot spots have the contradictively geometrical requirements for both the narrowest interstices to provide strong near-field coupling, and sufficient space to allow entrance of the analytes. Herein, a two-step method is employed to create hot spots within hybrid nanostructures, which consist of self-supported nanoporous gold films with the absorbed probes and subsequent nanoparticle conjugates without surface agents or mechanical motion. The molecules confined into 1 nm interstice exhibit 2.9×10^7 times enhancement in Raman scattering compared to pure nanoporous gold. Giant enhancement primarily results from strong near-field coupling between nanopore and nanoparticle, which is theoretically confirmed by finite-difference time-domain simulation. Excellent detection limits toward 10^{-11} mol l^{-1} offer an opportunity to track spatial orientation of single molecule and engineer hybrid nanostructures as commercial SERS substrates.

1. Introduction

Metal nanostructure films embedding hot spots are perfect substrates for surface enhanced Raman scattering (SERS) with considerable signal improvements.[1,2] Usually, hot spots confined within the interstices between the adjacent metal nanostructures are essential to enable single-molecule detection due to near-field coupling of localized surface plasmon resonance (LSPR).[3–8] Unfortunately, such substrates have competing geometrical requirements including the narrowest interstice between neighboring units to provide maximum near-field coupling, and sufficient space to accommodate the target probes.[9–13] Due to the exponential decay of electromagnetic fields normal to the metal surface, strong near-field coupling prefers to be obtained within the interstices with 1–2 nm separation.[14,15] On the other hand, such small gaps are not favorable for the insertion of target molecules dissolved in the solvents. Numerous efforts have been made to address these issues and different nanostructures including nanoparticles, nanowires, nanopores, and their conjugations have been used as the precursors.[16–20] Most fabrication processes utilize self-assemblies of colloidal suspensions stimulated either by mechanical motions or by modification of surface charge using surface agents.[16,18,21,22] While these films can provide enhanced Raman signals in certain sites, the enhancement factor strongly depends on specific parameters.[23–26] For instance, interstitial gap sensitively depends on the types and doses of surface agents rather than the probes of interest. Essentially, a primary concern is the random agglomeration of metal nanostructures due to non-specific electrostatic coalescence, an example being discrete nanoparticle clusters. Thus precise control of the interstices with narrow gaps is crucial to guarantee reproducible Raman scatterings. Herein, we fabricate hybrid nanostructure that addresses the issues discussed above and exhibits giant enhancement in Raman scattering. It consists of nanoporous gold (NPG) films decorated by gold nanoparticles that provide extremely narrow interstitial spaces contributing to significant near-field coupling and enhance Raman scattering by several orders of magnitude, enabling single-molecule detection.

2. Experimental procedures

2.1 Fabrications of gold nanoparticles and nanoporous gold

Gold nanoparticles with a size of 13 nm were prepared by chemical reduction of gold salt. 20 ml solution of 1.0 mM $HAuCl_4$ was heated to boil with persistent stirring of a magnetic bar, and 2 ml of 38.8 mM $Na_3C_6H_5O_7$ was subsequently added. Distilled water was supplied into the boiling mixture in order to keep total volume constant and control the gold nanoparticle concentrations. The solutions turned deep red after 10 min, the heater was turned off and the mixture was cooled to room temperature. NPG film with a thickness of 100 nm was synthesized by chemically etching a $Ag_{65}Au_{35}$ leaf, and was transferred onto silicon sheets. After drying under vacuum for two days, they were dipped into the 4-mercaptopyridine (4-MP) solutions (4-MP molecules were dissolved into ethanol) with the desired concentrations and were taken out promptly after wetting because the 4-MP solution can easily penetrate the hollow channel within 5 s. NPG film was immersed into the solution for a short time to avoid the formation of monolayer molecules on the gold surface. A NPG-adsorbent complex dried in a vacuum was immersed into gold colloids with the desired concentrations and taken out immediately, ensuring that most absorbed 4-MP molecules were not dissolved into colloidal suspensions. Most NPG films were tightly adhered with silicon sheets, which were used for scanning electron microscopy (SEM) characterization and Raman spectrum measurements. The peeled NPG films floating on the colloidal suspensions were immediately

[a]*Nevada Nanotechnology Center, Howard R. Hughes College of Engineering, University of Nevada, Las Vegas, Nevada, 89154-4026, USA*
[b]*Department of Physics, Xiamen University, Xiamen, 361005, China*
† Electronic supplementary information (ESI) available: SEM images of NPG-nanoparticles conjugates, SEM images of single layer gold nanoparticles, the spectra for calculating Raman enhancement, and Raman band assignments. See DOI: 10.1039/c0jm00884b

transferred onto carbon-coated copper grids for transmission electron microscopy (TEM) observation after spontaneous evaporation of the trapped solvent within the hollow channels.

2.2 Microstructural characterizations

TEM and SEM characterizations were conducted by TECNAI G^2 F30 transmission electron microscopy and JEOL 7500F scanning electron microscopy, respectively. Raman spectra were detected by a LabRAM HR Raman microscope manufactured by Horiba-Jobin-Yvon Inc. The 784.8 nm laser with a power of 1.5 mW had a beam size of 1 μm. Acquisition time was 20 s for each spectrum.

2.3 Computer simulation

In three-dimensional finite difference time domain (FDTD) simulations, the unit cell was defined as $0.25 \times 0.25 \times 0.25$ nm^3. The number of periods of the incident sinusoidal plane wave was set to 10 to guarantee calculation convergence, which could be judged by checking whether near zone electric field values had reached a steady state.[20] The sinusoidal plane wave had an amplitude of 1 V m^{-1}, and an irradiation wavelength of 784.8 nm.

3. Results and discussion

3.1 Characterization of hybrid nanostructures

Pure NPG film consists of interconnected gold ligaments and nanopores in three dimensions.[27] An SEM image, shown in Fig. 1(a), illustrates that most ligaments and nanopores exhibit elongated geometries in one direction, with a relatively uniform width of about 35 nm in the other vertical direction. All the ligaments have curved surfaces, representing spatial networks with random stacking. To enhance their SERS properties, gold colloids are introduced to partially fill in the hollow channels of the NPG film with prior absorption of the probe molecules. Spontaneous evaporation of the trapped solvent within nanoporous channels can create tiny interstices within these hybrid films as active sites for Raman scattering. Gold colloids with different concentrations were used to vary the density of gold nanoparticles on NPG film. As expected, reliable control of densities could be achieved as can be seen in SEM micrographs in Fig. 1(b) and 1(c). Our investigations show that the nanoparticle density within nanoporous channels is primarily dependent on colloidal concentration. It is also observed that gold nanoparticles are uniformly distributed into the nanopores of NPG films in low magnification SEM images (see Fig. S1, ESI†). The detailed configurations near the junctions between nanopores and nanoparticles can be roughly clarified by TEM as shown in Fig. 2. Low magnification image in Fig. 2(a) indicates that most gold nanoparticles randomly occupy partial volumes of the nanopores. Because of the complex hollow channels in three dimensions, specific stacking features cannot be precisely characterized except for their tiny gaps between nanopores and nanoparticles. The TEM image in Fig. 2(b) shows an individual 13 nm gold nanoparticle anchored onto the edge of a nanopore with 1 nm separation.

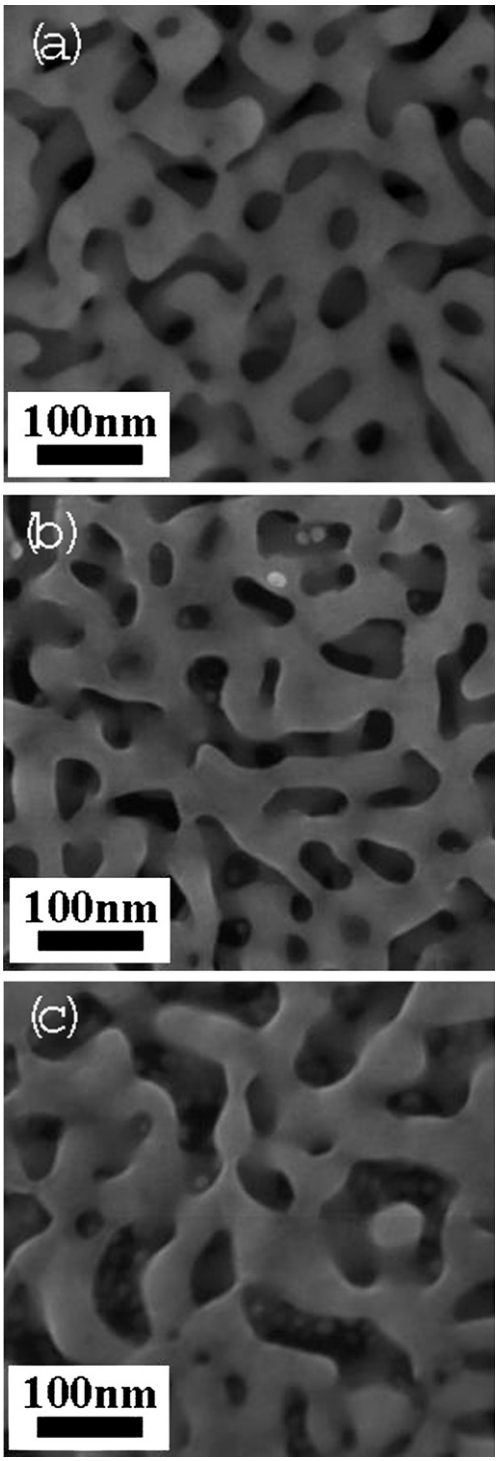

Fig. 1 Representative SEM images of pure NPG film (a), and NPG–nanoparticle conjugates by dipping NPG film into gold colloids with variable densities of 1×10^{11}/ml (b) and 1.6×10^{12}/ml (c).

3.2 SERS performance

A 10^{-4} M 4-MP solution was selected to initially evaluate SERS performance of both a NPG film and NPG–nanoparticle conjugates as shown in Fig. 3(a). For NPG film (concentration = 0), the available Raman band at 1097 cm^{-1} is extremely weak, which is designated as 12 a_1 trigonal ring breathing with C = S (the

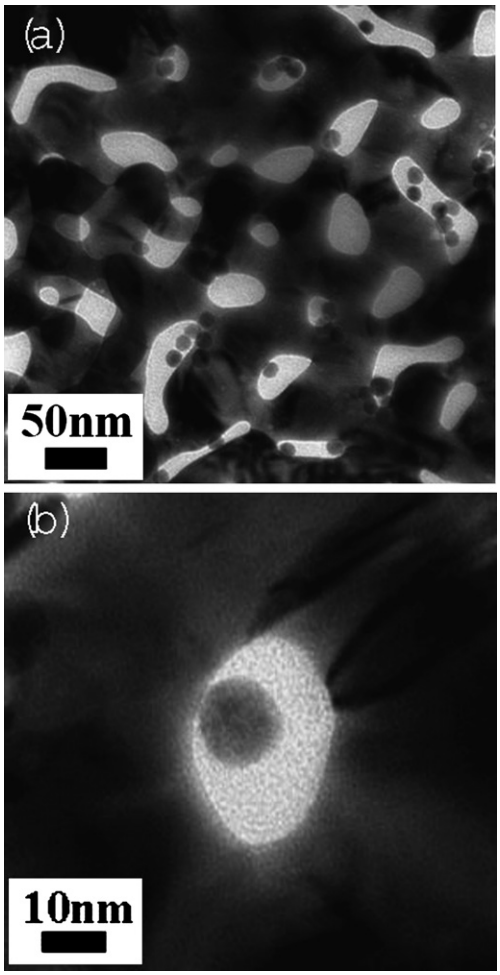

Fig. 2 (a) Low magnification TEM image of pure NPG–nanoparticle conjugates by immersing NPG film into gold colloids with 1.6×10^{12}/ml. (b) TEM image of an individual gold nanoparticle with a size of 13 nm conjugated to the nanopore with an interstitial gap of 1 nm.

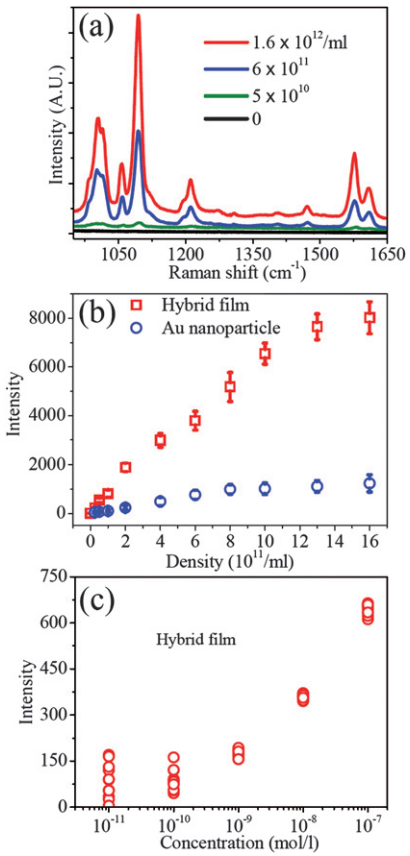

Fig. 3 (a) Typical SERS spectra on pure NPG film and NPG–nanoparticle conjugates. (b) Variation of Raman intensity at 1097 cm^{-1} with colloidal concentration, measured at ten different spots of the NPG–nanoparticle structures. Raman intensities acquired from monolayer of gold nanoparticles with various concentrations are included for comparison. (c) Raman intensity on NPG-nanoparticle conjugates varies with a concentration of 4-MP solution.

detailed assignments of Raman bands are listed in Table S1†).[28] In comparison, a remarkable Raman enhancement is obtained from NPG–nanoparticle conjugates, which significantly relies on the coverage of gold nanoparticles as shown in Fig. 3(b). One can consider this band as the reference, and the intensity monotonically increases with nanoparticle concentration in gold colloids.

Raman enhancement on hybrid NPG–nanoparticle films can probably arise from two different sources: near-field couplings within the interstices between nanopores and nanoparticles, or between adjacent nanoparticles. To determine their distinct contributions to Raman enhancements, SERS properties of gold nanoparticles were carried out (without the NPG film). A monolayer of gold nanoparticles with different densities was deposited on silicon substrates for SERS measurements (see Fig. S2, ESI†). Raman scattering from substrates with different nanoparticle densities, as shown in Fig. 3(b), exhibit very small variation. It thus implies that Raman enhancement on NPG–nanoparticle conjugates results from near-field coupling between nanopores and nanoparticles primarily rather than from adjacent nanoparticles embedded in hybrid films. Another evidence to confirm this is the superior detection limit of the NPG–nanoparticle conjugates compared to monolayer nanoparticles. Typical Raman spectra from NPG–nanoparticle conjugates with different 4-MP solutions are collected. As expected, Raman intensity decreases with decreasing concentrations, and available signal can be found when 10^{-11} M solution is employed. By contrast, Raman scattering from monolayer nanoparticles could not be observed for 10^{-9} M or less 4-MP solutions, which is three orders of magnitude less sensitive than for NPG–nanoparticle conjugates. Interestingly, Raman intensities from NPG–nanoparticle conjugates show the increased spatial inhomogenity for more dilute solutions, as confirmed by Raman measurements at different spots. Fig. 3(c) shows the concentration-dependence of Raman intensity measured at ten different spots showing more scattering intensity for 10^{-10} and 10^{-11} M 4-MP solutions. It is expected that the solutions with lower concentrations provide more non-uniform coverage compared to higher concentrations.

As described above, excellent sensing abilities of hybrid NPG–nanoparticle film originate from the introductions of numerous interstices. Some of them can serve as hot spots with huge Raman enhancements, enabling single-molecule detection. Fig. 4(a) shows a representative Raman spectra from a constant spot at variable acquisition times, evidencing that the probed molecule

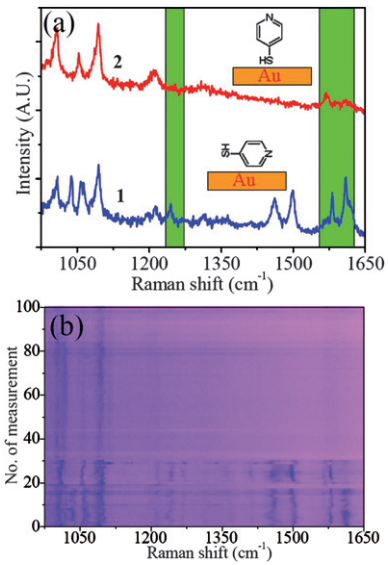

Fig. 4 (a) Raman spectra of NPG–nanoparticle conjugate evolving with irradiation time from initial orientation (1) to orientation (2) after irradiation. The detected solution concentration is 10^{-10} M. (b) Time evolution (number of measurements) of single-molecule spectra acquired from the same spot for 100 times.

within hot spot changes its orientation during laser irradiation. 4-MP molecules are initially oriented with the pyridine ring parallel to metal surface, as clearly identified by the existence of in-plane N–H mode at 1247 cm^{-1} as shown in curve 1.[28] After laser illumination, its diminished intensity, as shown in curve 2, implies that the N–H bond has an out-of-plane position. That is to say, the 4-MP molecule tends to have a postural evolution from the horizontal to perpendicular orientation after laser irradiation. The other evidence is a pyridine ring stretch with deprotonated and protonated nitrogen modes at 1586 and 1610 cm^{-1}. Initially, the pyridine ring is parallel to the gold surface, and a close distance between N atom and gold surface provides the dominant contributions to these two bands, so that strong Raman scattering as shown in curve 1 can be collected,[29,30] while their eliminated intensities corresponding to the obvious shifts to lower frequencies in curve 2 indicate that the charge transfer between gold and absorbed molecules in perpendicular orientation becomes weaker.[31,32] Fig. 4(b) illustrates complete evolutions of Raman spectra with time (number of measurements), indicating that the initial orientation of the 4-MP molecules does not revert from the perpendicular position even after 100 measurements. Usually Raman spectra from hot spots change with the polarization direction of incident irradiation.[3,5] Unfortunately, the repeatable results were not obtained to confirm molecular orientations in this work. In a technical aspect, it is significantly limited by surface geometries of the metal objects creating hot spots. Nanoporous gold is a three dimensional nanostructure with randomly stacked ligaments, which are different from gold nanpoparticles with nearly identical surface morphology.[33] LSPR of an individual ligament or LSPR coupling between nanopore and nanoparticle with a function of the polarization direction should be very complicated. On the other hand, numerous nanopore–nanoparticle conjugates as shown in Fig. 2(a) are observed within the exposed areas of laser irradiation (~1 μm in diameter). Therefore, different from the nanoparticle pair,[3] there are some difficulties to characterize the spatial configuration of hot spots in these hybrid nanostructures and clarify their intrinsic relationships between polarization direction and molecular orientation.

To quantify enhancement factors, *EF*, of hot spots within hybrid NPG–nanoparticle film, a 0.3 M 4-MP solution is employed as the bulk solution[34]

$$EF = (I_{SERS}N_{bulk})/(I_{bulk}N_{SERS})$$

where I_{SERS} and I_{bulk} are Raman intensities on hybrid NPG–nanoparticle film and from a 0.3 M 4-MP solution, respectively (see Fig. S3, ESI†). N_{SERS} and N_{bulk} are the corresponding molecular numbers. According to the optical configuration of the applied microscope, focal depth and beam size are 15 and 1 μm, respectively. In this study, the dried nanoporous film supported by a silicon substrate is dipped into the 4-MP solution and taken out immediately, which avoids the self-assembly of monolayer molecules onto the gold ligament. Therefore, molecular number in hybrid NPG–nanoparticle film can be roughly estimated by the volume of the trapped solvent within nanoporous channels multiplied by its concentration. If the band at 1097 cm^{-1} is selected as the reference, the *EF* of the NPG–nanoparticle conjugates is about 1.5×10^{13}, which is 2.9×10^{7} times larger than pure NPG film (5.1×10^{5}). It must be noted that *EF* values with 2–3 times difference can be obtained by selecting different bands that are available in two samples, which probably correlate with molecular orientations and charge transfer between metal surface and adsorbed molecules as well. Obviously, these distinctions are much smaller than the magnitudes from pure nanoporous gold and nanoporous gold–nanoparticle conjugates, and do not affect main intrinsic mechanism of Raman enhancement.

3.3 Simulation of electromagnetic field distribution

FDTD simulations were conducted to estimate field distributions of an individual nanopore and nanopore–nanoparticle pair as shown in Fig. 5.[20] As a result of near-field coupling between nanopores and nanoparticles, the maximum electromagnetic field confined in the interstices have 19 times enhancement if a single nanopore is selected as the reference. Fourth power of

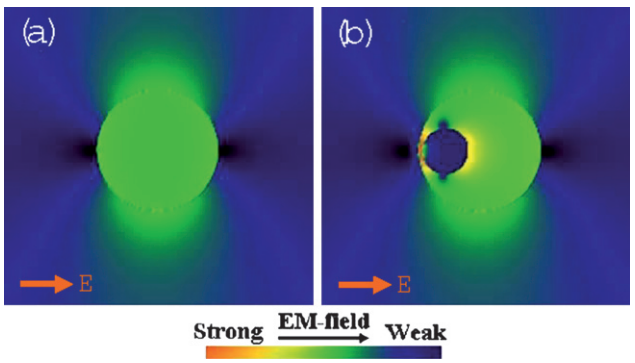

Fig. 5 Plane-view simulated electromagnetic field distributions of (a) an individual 35 nm diameter nanopore, and (b) an individual nanopore–nanoparticle pair.

field enhancement indicates a 1.3×10^5 times Raman enhancement on the nanopore–nanoparticle pair in comparison with an individual nanopore. This estimated value is about 200 times smaller than the experimental value, which probably results from chemical enhancement or anisotropic geometries of nanopores in the NPG film. Interestingly, the maximum electromagnetic field of the nanoparticle pair with a gap of 1 nm is about one-fifth of the maximum field corresponding to a nanopore–nanoparticle pair, which agrees with lower Raman intensity and a worse detection limit of monolayer nanoparticles observed experimentally. These evidences theoretically confirm that giant enhancement of Raman scattering on NPG–nanoparticle conjugates primarily originates from stronger near-field coupling between the nanopore and nanoparticle rather than nanoparticle–nanoparticle components.

3.4 Optimizing strategies in the future

Intrinsically, single-molecule detection depends on two key factors: the gap distance and laser polarization matching with the adjacent nanostructures.[3–5] The two-step method employed in this work can produce a large amount of tiny gaps with 1 nm separation, which can guarantee a strong near-field coupling of surface plasmon resonance from a nanopore and nanoparticles and higher SERS properties as well. Compared to NPG with refined pores,[12] a hybrid NPG–nanoparticle film is the efficient SERS substrate with much higher sensitivity. On the other hand, three-dimensional skeletons of NPG are random, so that gold nanoparticles are attached onto the surface with random orientations. Therefore, only small fraction of nanopore–nanoparticle pairs have a symmetrical axial parallel to the polarization direction of the incident laser, which makes the dominant contributions to high Raman scattering within hot spots. Obviously, NPG–nanoparticle conjugates with higher nanoparticle densities can improve the opportunity to find hot spots. The hint behind this will stimulate the fabrications of metal nanostructures consisting of vertically penetrated nanopores arrays with rectangular and triangle shapes in the forthcoming investigations, which will assist the coherent conjugations of most nanoparticles onto the parallel surfaces (sidewalls of nanopores). Essentially, a greater opportunity to find hot spots in specific laser polarization should be achieved (two directions for rectangular shape and three for triangle), which probably improve the reliabilities and sensitivities of hybrid nanopore–nanoparticles for single-molecule detection.

4. Conclusions

Hybrid nanopore–nanoparticle films consisting of self-supported nanoporous gold with pre-absorbed molecules and the subsequent nanoparticle conjugation are fabricated as a SERS substrate with embedded hot spots. Raman scattering collected from hot spots with a gap of 1 nm exhibits 2.9×10^7 augments in comparison with pure nanoporous gold without any nanoparticle conjugations. An excellent detection limit towards 10^{-11} mol l^{-1} and a giant enhancement factor of 1.5×10^{13} dominantly result from the tremendous LSPR coupling between the nanopore and nanoparticle, which offers the opportunity to track spatial orientation of single molecule within hot spots and confirmed by the simulated field distributions within the tiny gap. The creation of the tiny gaps with comparable scales of the trace molecules independent on the application of surface agents and mechanical motion has the advantage to be utilized as the commercial sensor with high sensitivities.

References

1 M. E. Stewart, C. R. Anderton, L. B. Thompson, J. Maria, S. K. Gray, J. A. Rogers and R. G. Nuzzo, *Chem. Rev.*, 2008, **108**, 494.
2 M. J. Banholzer, J. E. Millstone, L. D. Qin and C. A. Mirkin, *Chem. Soc. Rev.*, 2008, **37**, 885.
3 S. M. Nie and S. R. Emery, *Science*, 1997, **275**, 1102.
4 K. Kneipp, Y. Wang, H. Kneipp, L. T. Perelman, I. Itzkan, R. Dasari and M. S. Feld, *Phys. Rev. Lett.*, 1997, **78**, 1667.
5 H. X. Xu, E. J. Bjerneld, M. Käll and L. Borjesson, *Phys. Rev. Lett.*, 1999, **83**, 4357.
6 A. M. Michaels, J. Jiang and L. Brus, *J. Phys. Chem. B*, 2000, **104**, 11965.
7 Z. Wang and L. J. Rothberg, *J. Phys. Chem. B*, 2005, **109**, 3387.
8 L. H. Qian, W. Shen, B. Das, B. Shen and G. W. Qin, *Chem. Phys. Lett.*, 2009, **479**, 259.
9 Z. Wang, S. Pan, T. D. Krauss, H. Du and L. J. Rothberg, *Proc. Natl. Acad. Sci. U. S. A.*, 2003, **100**, 8638.
10 Y. Lu, G. L. Liu and L. P. Lee, *Nano Lett.*, 2005, **5**, 5.
11 D. R. Ward, N. K. Grady, C. S. Levin, N. J. Halas, Y. P. Wu, P. Nordlander and D. Natelson, *Nano Lett.*, 2007, **7**, 1396.
12 L. H. Qian, X. Q. Yan, T. Fujita, A. Inoue and M. W. Chen, *Appl. Phys. Lett.*, 2007, **90**, 153120.
13 L. H. Qian and M. W. Chen, *Appl. Phys. Lett.*, 2007, **91**, 083105.
14 C. L. Haynes, A. D. McFarland, L. L. Zhao, R. P. Van Duyne, G. C. Schatz, L. Gunnarsson, J. Prikulis, B. Kasemo and M. Käll, *J. Phys. Chem. B*, 2003, **107**, 7337.
15 Q. Yu, P. Guan, D. Qin, G. Golden and P. M. Wallace, *Nano Lett.*, 2008, **8**, 1923.
16 A. Tao, F. Kim, C. Hess, J. Goldberger, R. R. He, Y. G. Sun, Y. N. Xia and P. D. Yang, *Nano Lett.*, 2003, **3**, 1229.
17 A. J. Haes, C. L. Haynes, A. D. McFarland, G. C. Schatz, R. P. Van Duyne and S. Zou, *MRS Bull.*, 2005, **30**, 368.
18 S. J. Lee, A. R. Morrill and M. Moskovits, *J. Am. Chem. Soc.*, 2006, **128**, 2200.
19 S. O. Kucheyev, J. R. Hayes, J. Biener, T. Huser, C. E. Talley and A. V. Hamza, *Appl. Phys. Lett.*, 2006, **89**, 053102.
20 H. Wei, U. Håkanson, Z. L. Yang, F. Höök and H. Xu, *Small*, 2008, **4**, 1296.
21 D. M. Kuncicky, B. G. Prevo and O. D. Velev, *J. Mater. Chem.*, 2006, **16**, 1207.
22 D. Graham, D. G. Thompson, W. E. Smith and K. Faulds, *Nat. Nanotechnol.*, 2008, **3**, 548.
23 R. G. Freeman, K. C. Grabar, K. J. Allison, R. M. Bright, J. A. Davis, A. P. Guthrie, M. B. Hommer, M. A. Jackson, P. C. Smith, D. G. Walter and M. J. Natan, *Science*, 1995, **267**, 1629.
24 H. Wang, C. S. Levin and N. J. Halas, *J. Am. Chem. Soc.*, 2005, **127**, 14992.
25 Y. Fang, N. H. Seong and D. D. Dlott, *Science*, 2008, **321**, 388.
26 S. Liu and Z. Tang, *J. Mater. Chem.*, 2010, **20**, 24.
27 F. Yu, S. Ahl, A. M. Caminade, J. P. Majoral, W. Knoll and J. Erlebacher, *Anal. Chem.*, 2006, **78**, 7346.
28 F. R. Dollish, W. G. Fateley and F. F. Bentley, *Characteristic Raman frequencies of organic compounds*, John Wiley & Sons: New York, 1974.
29 J. Baldwin, N. Schuhler, I. S. Butler and M. P. Andrews, *Langmuir*, 1996, **12**, 6389.
30 Y. W. Cao, Q. Zhou, Y. Li, Y. R. Yan, Y. Wu and J. W. Zheng, *J. Phys. Chem. C*, 2007, **111**, 16990.
31 J. W. Hu, B. Zhao, W. Q. Xu, B. F. Li and Y. G. Fan, *Spectrochim. Acta, Part A*, 2002, **58**, 2827.
32 T. Shegai, A. Vaskevich, I. Rubinstein and G. Haran, *J. Am. Chem. Soc.*, 2009, **131**, 14390.
33 T. Fujita, L. H. Qian, K. Inoke, J. Erlebacher and M. W. Chen, *Appl. Phys. Lett.*, 2008, **92**, 251902.
34 W. B. Cai, B. Ren, X. Q. Li, C. X. She, F. M. Liu, X. W. Cai and Z. Q. Tian, *Surf. Sci.*, 1998, **406**, 9.